

Effects of initial up-warp deformation on the stability of the CRTS II slab track at high temperatures^{*}

Zui CHEN^{1,2}, Jie-ling XIAO^{†‡1,2}, Xiao-kai LIU^{1,2}, Xue-yi LIU^{1,2}, Rong-shan YANG^{1,2}, Juan-juan REN^{1,2}

¹MOE Key Laboratory of High-speed Railway Engineering, Southwest Jiaotong University, Chengdu 610031, China

²School of Civil Engineering, Southwest Jiaotong University, Chengdu 610031, China

[†]E-mail: xjling@swjtu.cn

Received Mar. 12, 2018; Revision accepted Sept. 7, 2018; Crosschecked Nov. 27, 2018

Abstract: Initial up-warp deformation is one of the key factors that affect the stability of the China Railway Track System type II (CRTS II) slab track. Through modeling analysis, we studied the effects of different initial up-warp conditions on the deformation and stability of a slab track at high temperatures. Based on the theory of ‘variable span length’ in continuous welded rail (CWR), a vertical stability analysis model of the CRTS II slab track was established using the finite element method (FEM), and a scale model test was conducted. The effects of initial up-warp deformation features, such as rise displacement, span length, and line type on the stability of track slabs at high temperatures were studied through simulation. Results showed that the trends of vertical displacement were almost the same based on the FEM, analytical method, and on-site testing, but there was a better agreement between results from the FEM and the analytical method. When the span length was 6.5 m and the rise displacement of the initial up-warp reached 15 mm, compressional destruction was most likely to occur on the concrete at the bottom of the apex. The rise-span ratio of the slab up-warp reached its maximum when the initial up-warp span was 6.5 m at high temperatures. It is easier for track slabs to maintain their original form at a high temperature when there is an angle at the apex or a smooth boundary. However, with a smooth boundary, the concrete at the bottom of the apex is more likely to suffer compressional destruction. Therefore, to ensure the stability of the CRTS II slab track, an initial up-warp with a span of 6.5 m and a rise of 15 mm should be avoided, and the effects of different line types of the initial up-warp also need to be considered.

Key words: High-speed railway; China Railway Track System type II (CRTS II) slab track; Initial up-warp; High temperature; Stability

<https://doi.org/10.1631/jzus.A1800162>

CLC number: U213.2

1 Introduction

In recent years, high-speed railways have been widely developed in China (Fang, 2011; Tan et al., 2016; Zhang et al., 2017). As one of the main track structures of a high-speed railway, the China Railway Track System type II (CRTS II) slab track was introduced and reformed based on the German Bögl

slab. This kind of track was first put into operation in the Beijing-Tianjin intercity passenger lines in 2008. Because of high precision and durability, it was then widely applied to other routes in China, including the Beijing-Shanghai, Shanghai-Hangzhou, and Shijiazhuang-Wuhan lines (Liu et al., 2010; Yan et al., 2015; Long et al., 2018).

The main components of the CRTS II slab track are the CN60 rail (Chinese standard rail with a mass of 60 kg/m) (Tao et al., 2017), elastic fastening system type WJ-8 invented in China, track slabs, cement asphalt mortar (CA mortar), and a hydraulic material layer. A cross section of a CRTS II slab track is shown in Fig. 1. Track slabs comprise prefabricated concrete slabs made of reinforced concrete (0.2-m

[‡] Corresponding author

^{*} Project supported by the National Natural Science Foundation of China (Nos. U1434208, 51678506, U1534203, 51578472, and 51778543)

 ORCID: Zui CHEN, <https://orcid.org/0000-0001-9317-0591>; Jie-ling XIAO, <https://orcid.org/0000-0002-4692-7464>

© Zhejiang University and Springer-Verlag GmbH Germany, part of Springer Nature 2018

thick, 2.55-m wide, and 6.45-m long). The slabs are connected by wide-narrow joints consisting of turn-buckles and elastic concrete mortar to form a longitudinal continuous track (Lichtberger, 2005). Wide-narrow joints are the weak parts of the CRTS II slab track, and are constructed by post-cast concrete after the track slabs are longitudinally coupled. The wide joint is 0.2 m, and the narrow joint 0.05 m wide (Fig. 2). Compared to prefabricated concrete slabs, wide-narrow joints are more prone to be damaged such as cracking and breakage, leading to an eccentric pressure state causing up-warp in the track slab (Gao et al., 2016).

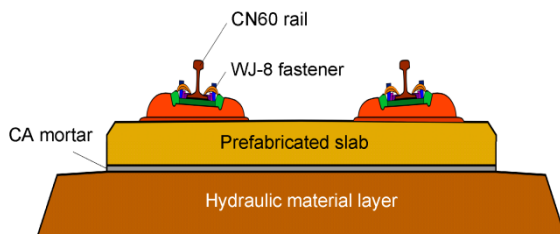


Fig. 1 A cross section of a CRTS II slab track

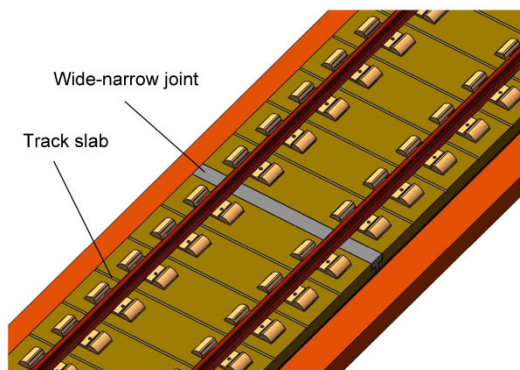


Fig. 2 A wide-narrow joint in a CRTS II slab track

Track slabs and the hydraulic material layer are bonded together by the bonding behavior of the CA mortar. However, the mortar layer has a limited vertical restraint ability on the track slabs. De-bonding of track slabs and the mortar layer can easily occur because of extensive construction, changeable foundations, structural deterioration under aging effects, and other factors (Han et al., 2015). There is a huge temperature force in track slabs, especially in high-temperature environments. Due to temperature gradients and the periodicity of the track structure, wide-narrow joints are easily destroyed, breaking the stress uniformity in track slabs, leading to their de-bonding

(Zhang and Zhao, 2018). In addition, in rainy environments, if the track structures lack of maintenance, water erosion will occur in the mortar layer between the track slabs and the hydraulic material layer, due to the effects of long-term vehicle load and environmental factors. In poorly drained routes, large amounts of water will seep into the mortar layer, leading to a deterioration in the mechanical properties of track slabs, which can also cause de-bonding between the layers (Cao et al., 2016). These factors could easily lead to initial up-warp deformation of track slabs. At extremely high temperatures, these factors would trigger further up-warp displacement, and increase the risk of systematic instability (Liu et al., 2015; Liu and Feng, 2016). Through on-site investigations of CRTS II slab tracks in East China, the phenomenon of up-warps is known to occur on track slabs in summer due to the effect of high temperatures (Fig. 3). In some severely damaged route segments, the vertical displacement is higher than 10 mm, far more than the upper limit of 2 mm for track irregularity (Wei, 2014). Therefore, up-warp of track slabs will affect the safety of vehicle operation. The problems of CRTS II slab tracks greatly threaten the quality and safety of high-speed vehicle operation, and have aroused widespread concern.



Fig. 3 Track slab up-warp on site

The buckling of longitudinal continuous structures was analyzed initially using the Euler column model, and the critical load can be found by the balance method or the defect method (Ziegler, 1977; Shahba and Rajasekaran, 2012). Zhou and Dai (2015) studied the stability of a CRTS II track slab on simply supported girder bridges. They concluded that the track structure cannot be regarded as an ideal Euler column model, and the actual nonlinearity between

layers should be considered. Yang et al. (2015) and Ren et al. (2017) came up with a calculation formula for the critical temperature force of track slabs by energy norm, referring to the model of ‘equivalent span length’ in continuous welded rail (CWR). However, differences in span length between the initial up-warp and further up-warp were ignored. Also, the effect of the line type of the initial up-warp on the stability of the track system was not thoroughly studied. Previous studies on the stability of CWR have a great reference value for analysis of the stability of CRTS II slab tracks. Kish et al. (1982) discussed the lateral, longitudinal, and torsional resistances of CWR in detail and used statistical methods to evaluate the safety of buckling. Lin et al. (2003) considered the geometrical nonlinearities of the rail and the material nonlinearity of ballasts, and discovered that a 2D rail-sleeper model has a higher structural stability than a 3D model. Rybkin et al. (2013) studied the stability of the CWR in small-radius curves. Zhang and Chen (2007) and Martinez et al. (2015) applied the balance method of internal and external moment to derive a formula for calculating the stability of CWR.

Due to quality restriction in track construction and structural characteristics, track slabs have different span lengths and up-warp rise displacements, and line types have not been considered. Therefore, a more thorough study on the effects of initial up-warp status on the stability of the track structure is of great significance to the operation and maintenance of the track system.

2 Analysis theory of CRTS II slab track up-warp

According to the structural characteristics of the CRTS II slab track (Liu et al., 2010), the following assumptions were made:

1. Track slabs are simplified as beam elements, ignoring the lateral effect of the track structure.
2. The structure is considered only in the elastic weighted range, and the bonding strength of the mortar layer on the track slabs is ignored.
3. The constraints of the rail and fastener system on the stability of the track slab are ignored.

Yang et al. (2015) and Ren et al. (2017) derived a

calculation formula for the critical temperature force on the basis of the theory of ‘equivalent span length’ in CWR, assuming that the span length of further up-warp is equal to that of the initial up-warp, which differs from the actual status on site. Therefore, cases of different span lengths should be considered. As the track slab is a longitudinal continuous structure, the span length will change during the up-warp process. Therefore, initial and further up-warp curves (y_0 and y) are set separately. As shown in Fig. 4, y_0 and y are both set without angles at the boundary, that is, as half-wave quadratic sine curves with a continuous first derivative.

In Fig. 4, f_0 and l_0 are the rise displacement and span length, respectively, of the initial up-warp, and f and l are the rise and span length of further up-warp. The axial deformation Δl ($\Delta l = \Delta l_T - \Delta l_0$, where Δl_0 and Δl_T represent the differences in arc length before and after up-warp deformation, respectively) is the change in the arc length (not the span length) of track slabs affected by the temperature force P . ds_0 and ds_T are the differentials of arc length before and after up-warp deformation, respectively. According to Fig. 5, Δl can be expressed as follows:

$$\begin{aligned} \Delta l &= \int_{-l/2}^{l/2} \left[\left(\frac{ds_T}{dx} - dx \right) - \left(\frac{ds_0}{dx} - dx \right) \right] dx \\ &= \int_{-l/2}^{l/2} \left[\sqrt{1 + ((y+y_0)')^2} - \sqrt{1 + (y_0')^2} \right] dx. \end{aligned} \quad (1)$$

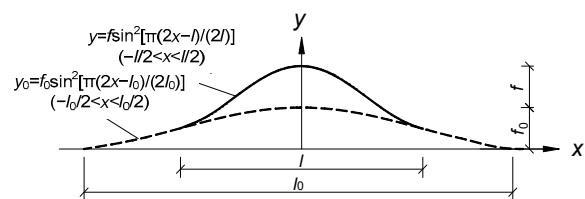


Fig. 4 Assumption of deformed curves

During the up-warp process, the total potential energy (U) of the track slabs consists of compressive deformation energy (U_1), bending energy (U_2), and gravitational potential energy (U_3).

In Eq. (2) (see the top of the next page), EI represents the flexural rigidity of track slabs, $M(x) = (EIy'')$ is the distribution of the bending moment in the track slabs during the up-warp process, and ρ , g , and A represent the concrete density, gravity acceleration, and sectional area of the track slabs, respectively.

$$\begin{aligned}
 U &= U_1 + U_2 + U_3 = -P\Delta l + \frac{1}{2EI} \int_{-l/2}^{l/2} (M(x))^2 dx + \int_{-l/2}^{l/2} y \rho g A dx \\
 &= -P \left\{ \frac{1}{2} \left(\frac{\pi f}{l} \right)^2 \int_{-l/2}^{l/2} \sin^2 \left(\frac{2\pi x}{l} \right) dx + \frac{1}{2} \frac{\pi^2 f f_0}{l l_0} \int_{-l/2}^{l/2} \left[2 \sin \left(\frac{2\pi x}{l} \right) \sin \left(\frac{2\pi x}{l_0} \right) \right] dx \right\} + \frac{2EI\pi^4 f^2}{l^4} \int_{-l/2}^{l/2} \sin^2 \left(\pi \frac{2x+l}{2l} \right) dx \\
 &\quad + \rho g A f \int_{-l/2}^{l/2} \sin^2 \left(\pi \frac{2x+l}{2l} \right) dx \\
 &= -P \left[\frac{(\pi f)^2}{4l} + \frac{\pi f f_0 l_0}{l_0^2 - l^2} \sin \left(\frac{l}{l_0} \pi \right) \right] + \frac{EI\pi^4 f^2}{l^3} + \frac{1}{2} \rho g A l f. \tag{2}
 \end{aligned}$$

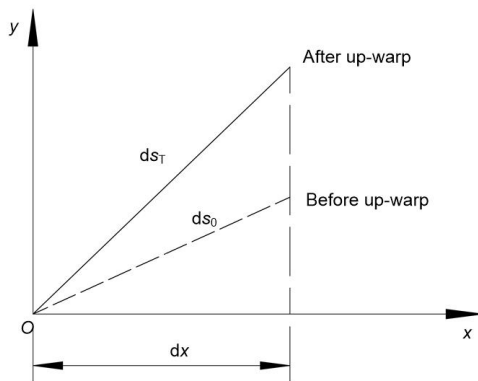


Fig. 5 Differences in the arc length of the track slabs before and after deformation

Based on the principle of energy norm (Reissner, 1946), take the partial derivative U with respect to f , that is, $\partial U / \partial f = 0$. Setting k as the ratio of l to l_0 , the expression of f is taken as

$$f = \frac{\frac{2k\pi \sin(k\pi)}{1-k^2} f_0 l^2 P - \rho g A l^4}{4EI\pi^4 - \pi^2 l^2 P}. \tag{3}$$

According to Eq. (3), if the line type of the initial up-warp of the track slab is stable, f is affected by f_0 , l_0 , and l . As the denominator approaches 0, f approaches infinity, and the buckling of the track slab can be determined. Setting l_{cr} as the span length when buckling, the expression of the critical load for buckling P_{cr} can be determined as

$$P_{cr} = \frac{4EI\pi^2}{l_{cr}^2}. \tag{4}$$

Eq. (4) shows that when vertical buckling occurs in the track slab, the effective length of P_{cr} is

equal to $0.5l_{cr}$ in the Euler column model. Although the location of the boundary point will change during the up-warp process, the boundary of the up-warp and extension part is still in a state without rotation. Therefore, it is the same to the situation with both ends fixed in the Euler buckling equation, and the track system can also be determined to be in the buckling state if $l=l_{cr}$.

Taking the partial derivative of l for f will result in $\partial f / \partial l = 0$. The relationship between l and l_0 can be determined from the implicit formula of $k(l, l_0)$ expressed as

$$\begin{aligned}
 &\left[\frac{\pi f_0 k P}{1-k^2} \left(\frac{3-k^2}{1-k^2} \sin(k\pi) + k\pi \cos(k\pi) \right) \right. \\
 &\quad \left. - 2\rho g A l^2 \right] (4EI\pi^2 - Pl^2) \\
 &\quad + Pl^2 \left(\frac{2\pi \sin(k\pi)}{1-k^2} f_0 k P - \rho g A l^2 \right) = 0. \tag{5}
 \end{aligned}$$

3 Calculation model and parameters

On account of the highly nonlinear nature of the model, analytical methods based on energy norm suit only idealized buckling analysis, and cannot accurately solve the problems above. Therefore, the finite element method (FEM) was adopted. A geometry model for vertical stability was established (Fig. 6), and the local FEM model is shown in Fig. 7.

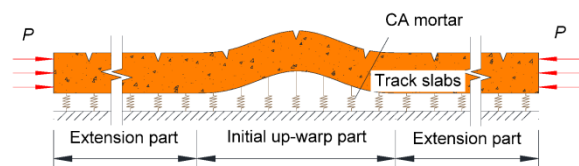


Fig. 6 Diagram of the geometry model

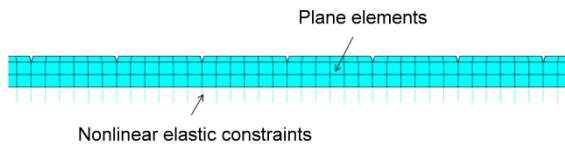


Fig. 7 Diagram of the local model for the finite element method (FEM)

As Fig. 6 shows, the model is made up mainly of track slabs and the CA mortar. As the effects of the hydraulic material layer, rail, and the fastener system on the stability of the track system are quite minor, they have been ignored in the FEM model. As Fig. 7 shows, first, track slabs are established as plane elements in the FEM model to describe the shape of pre-cracking joints. The units are established as rectangular elements with a size of 0.1 m with a high accuracy. Track slabs contain the initial up-warp part and the extension part. Because the boundary between the initial up-warp part and the extension part is in the intermediate state between hinged and fixed states during the up-warp process, and the location of the boundary point will change simultaneously, longitudinal extension parts of 100 m in length are established at both ends of the initial up-warp part to eliminate the boundary effect. Then due to the limited tensile strength of the mortar layer, the adhesion of the mortar layer is neglected. Therefore, to simulate the stiffness of the CA mortar, constraints between the track slabs and the hydraulic material layer are simplified to nonlinear constraints with a unidirectional compression function in the FEM model. The F - δ curve is obtained by equivalent conversion of the elastic modulus of CA mortar (Liu et al., 2010; Zhou and Dai, 2015), as shown in Fig. 8 (F is positive when the spring is subjected to drag force, and vice versa). Finally, a load of temperature rise ΔT is applied to simulate the warming effect of the track slab in a high-temperature environment. P is imposed at both ends to make the track slabs reach the balance of temperature force. If the up-warp process is in the stage of elastic deformation, it can be approximated as $P=E\alpha A\Delta T$, where E and α are the elastic modulus and the thermal expansion coefficient of the track slabs, respectively.

The main parameters of the model are shown in Table 1.

The arc-length method (Crisfield, 1982; Malardo and Alessandri, 2004) is used to calculate the

equilibrium path of ΔT and f , and the regulation for ΔT and f is shown roughly in Fig. 9 (Esveld, 2001). When ΔT reaches $T_{B,max}$, f bounces to point C if ΔT continues to increase. It can be determined that point B is a snapping point. Therefore, the track system is in an unstable state when ΔT reaches $T_{B,max}$. Thus, $T_{B,max}$ is a critical temperature rise ΔT_{cr} . The practice shows that ΔT in track slabs will not exceed 60 °C even

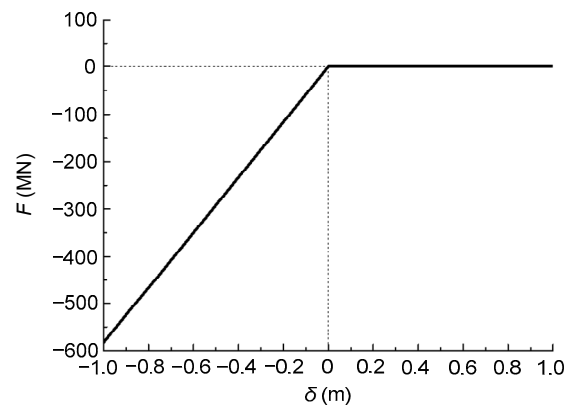


Fig. 8 F - δ curve of the mortar layer

Table 1 Main parameters of the model

Component	Parameter	Value
Track slab	Elastic modulus (MPa)	3.55×10^4
	Density (kg/m^3)	2400
	Poisson's ratio	0.20
	Thermal expansion coefficient ($^{\circ}\text{C}^{-1}$)	1.0×10^{-5}
	Width \times thickness (m \times m)	2.55×0.2
CA mortar	Elastic modulus (MPa)	7.0×10^3
	Thickness (m)	0.03
	Unidirectional compression stiffness (N/m)	5.83×10^8

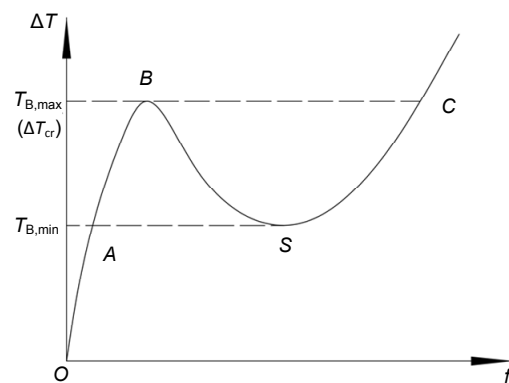


Fig. 9 ΔT - f curve of the track slabs

when exposed to extremely high temperatures. Typical situations for the initial span length equal to one slab and two slabs, that is, $l_0=6.5$ m and $l_0=13$ m are adopted. If the track slabs are not damaged, the values of ΔT_{cr} are as shown in Table 2. According to the results described in Section 5, when ΔT reaches 60°C , the concrete of the track slabs will be destroyed. Therefore, ΔT will not reach ΔT_{cr} unless the track slabs are destroyed.

Table 2 ΔT_{cr} values under different magnitudes of l_0 and f_0

l_0 (m)	ΔT_{cr} ($^\circ\text{C}$)		
	$f_0=10$ mm	$f_0=15$ mm	$f_0=20$ mm
6.5	95.2	80.7	71.9
13.0	108.1	88.7	74.5

4 Model verification

The reasonableness and usability of the model were verified by the analytical method described in Section 2 and a scale model test on site. A continuous track slab model with a size of $2200\text{ mm}\times 120\text{ mm}\times 10\text{ mm}$ was established with a scale ratio of 1:20 (Fig. 10). The test slab was made of aluminum with the parameters shown in Table 3. To simulate f_0 , a plate with a thickness of 1.5 mm was inserted into the bottom of the test slab.

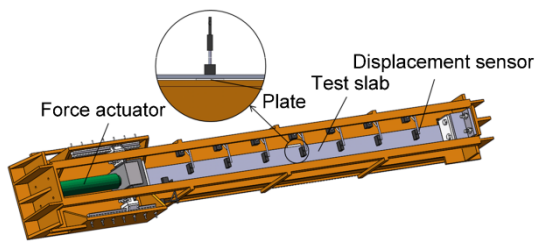


Fig. 10 Diagram of experimental tools

Table 3 Material parameters of aluminum board

Parameter	Value
Elastic modulus (MPa)	7.2×10^4
Density (kg/m^3)	2700
Poisson's ratio	0.33
Thermal expansion coefficient ($^\circ\text{C}^{-1}$)	2.3×10^{-5}

The load of ΔT was simulated by imposing an end force P , loaded from 0 kN to the buckling state,

and the force magnitude was monitored by a pressure sensor. Seven displacement sensors were arranged on the surface of the test slab to measure the vertical displacement. The measuring points were spaced at an interval of 0.275 m.

The results of vertical displacement distribution of the test slab obtained from the FEM, analytical method, and on-site test when the end force was loaded to 8 kN, are shown in Fig. 11.

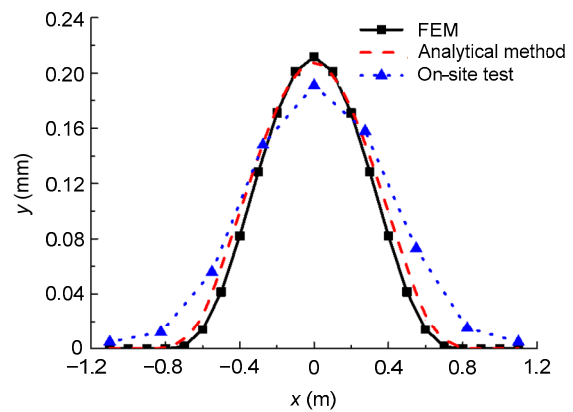


Fig. 11 Vertical displacement distribution of the test slab

According to Fig. 11, the maximum vertical displacement was in the middle of the slab, which can be certified as f . Under the action of P , the line type obtained by the FEM fits well with the half-wave quadratic sine curve assumed by the analytical method, and closely coincides with the result from the on-site test. Parameters and boundary conditions of the test on site were substituted into Eqs. (3)–(5) and the FEM model. Values of f with different magnitudes of P using the three methods are shown in Fig. 12.

Results show that the trends in f are almost the same for the three methods, but there is a better agreement between the results from the FEM and the analytical method. Values of P_{cr} for FEM (the equivalent force generated by ΔT_{cr} in Fig. 9), analytical method (Eqs. (3)–(5)), and test result (the buckling state) are 8.36 kN, 9.07 kN, and 9.45 kN (Fig. 12), respectively, under the condition of $f_0=1.5$ mm. The variation in f in the test result is a little larger when $P<7.8$ kN. However, the f error was maintained within the range of 0.1 mm in the stage of elastic deformation, and the P_{cr} error was almost within the range of 10%.

Therefore, it was verified that the FEM above can be used for further analysis of the stability of track slabs.

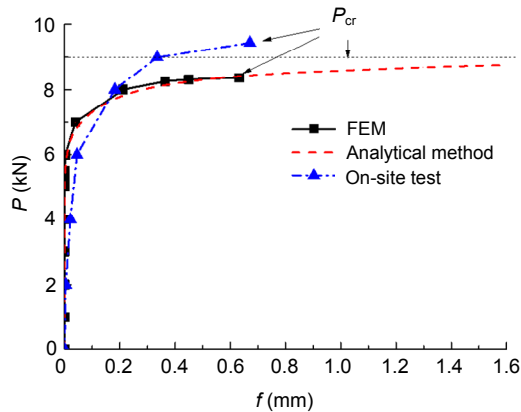


Fig. 12 Contrast of f under different magnitudes of P

5 Effects of initial up-warp of track slabs

5.1 Effects of f_0 on the stability of track slabs

Because of the effects of the construction environment of CRTS II slab tracks, f_0 will have different values on site. Affected by the length of prefabricated slabs, l_0 is usually the same to the length of a slab, and assumed to be 6.5 m. The practice shows that the f_0 values on site are larger than 10 mm in a severely damaged route; therefore, f_0 is taken as 1, 3, 5, 7.5, 10, 15, or 20 mm assuming that the line type of the initial up-warp is a half-wave quadratic sine curve. Static state responses of track slabs under the condition of ΔT from 0 °C to 60 °C were analyzed. The variation in f , the change in l , and $M(x)$ under the condition of $\Delta T=60$ °C are shown in Figs. 13–15, respectively. The moment is assumed to be positive when the bottom slab is under drag force.

Fig. 13 shows that the up-warp feature of the track slabs is closely related to f_0 . By increasing ΔT , the effect of f_0 on the stability of the track slabs becomes larger. When $\Delta T=60$ °C, the values of f are 2.1, 4.2, and 6.7 mm, under the condition that f_0 equals 10, 15, and 20 mm, respectively. However, there is almost no up-warp of the track slabs when $f_0=1$ mm. According to the manufacturing technology of track slabs in China (Zhao, 2010), the initial flatness is ± 0.3 mm, which is less than 1 mm. Therefore, early processes of construction and operation will not induce instability in the track system.

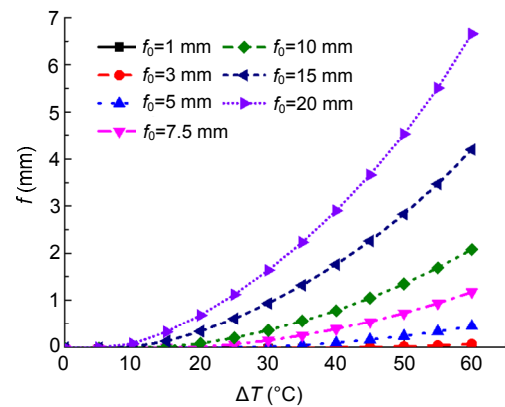


Fig. 13 Variation in f under different values of f_0

Fig. 14 shows that when ΔT reaches a certain value, l starts growing, due to the constraint of the gravitational field. There is a positive correlation between f_0 and l . When $\Delta T=60$ °C, the values of l are 6.4, 7.7, and 9.1 m, and the ratios (f/l) are 0.32, 0.54, and 0.74 mm/m when the values of f_0 are 10, 15, and 20 mm, respectively. Therefore, when f_0 is larger, it is more adverse to traffic safety.

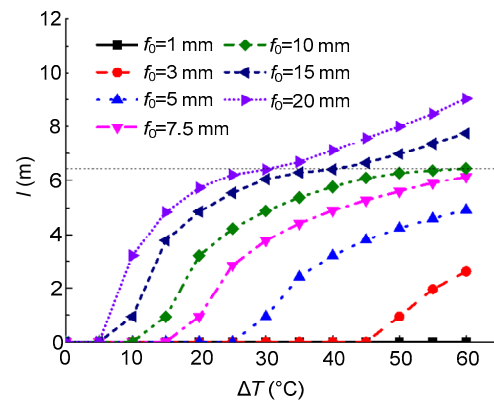


Fig. 14 Variation in l under different values of f_0

In addition, if the line type of the initial up-warp is a half-wave quadratic sine curve, when the track slabs begin to up-warp, l begins to bounce because of the temperature load. As the value of l approaches l_0 , the growth rate of l slows down. After l exceeds l_0 , the growth rate increases. Therefore, in the process of construction and operation of a CRTS II slab track, l should be kept within the length of l_0 to avoid a greater extent of de-bonding affecting the safety of high-speed vehicle operation.

Fig. 15 shows that under different values of f_0 , $M(x)$ changes obviously. With a minor value of f_0 (no

more than 3 mm), the apex of the span is restrained by the gravitational field, f is very small, and the bending moment of the initial span section is inconspicuous. When f_0 exceeds 3 mm, the bottom slab at the boundary of the span endures tension and the value tends to increase rapidly. The bending moment is set as M_a at the apex and M_b at the boundaries. With the appearance of up-warp, M_a becomes more obvious. Because the maximum bending moment occurs at the apex, with the up-warp of the track slabs, concrete stress at the apex is the most unfavorable. Through calculation, when ΔT is within 60 °C, under the combined action of temperature and pressure, the cross section of the track slabs is under compression. The compressive stress at the bottom slab of the apex is the largest. Therefore, a limit value of f_0 can be proposed based on the compressive stress at the bottom slab of the apex. The design value for concrete compressive strength of the C55 type concrete used for CRTS II slab tracks is 25.3 MPa in China. According to the calculation, when M_a exceeds 98.6 kN·m (i.e., when f_0 exceeds 15 mm), the concrete at the bottom slab of the apex is prone to compressive failure.

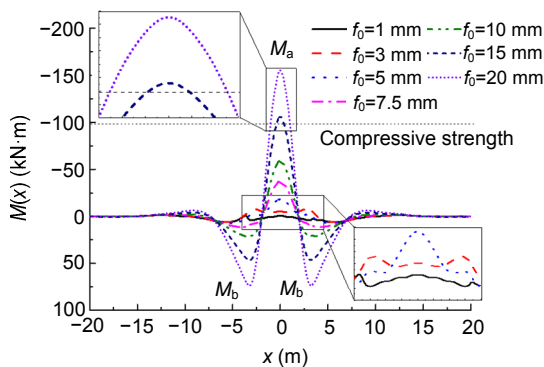


Fig. 15 Distribution of $M(x)$ under different values of f_0 ($\Delta T=60$ °C)

5.2 Effects of l_0 on the stability of track slabs

The value of l_0 varies on account of the complicated procedure of longitudinal construction and changeable foundations of CRTS II slab tracks. According to Fig. 15, the compressive stress at the bottom slab of the apex is closest to the design value of the compressive strength when $f_0=15$ mm. Therefore, $f_0=15$ mm is assumed in the following analysis. On-site studies have shown that l_0 falls mainly in the

range of 3–7 m. To further study the influence of l_0 on the stability of track slabs, the up-warp regulation was analyzed under the condition that l_0 equals 3, 5, 6.5, 8, 10, or 13 m. The results for f are presented in Fig. 16, and those for l in Fig. 17. Results for $M(x)$ under the condition of $\Delta T=60$ °C are shown in Fig. 18.

Fig. 16 shows that for different values of ΔT , different values of f correspond to different values of l_0 . When ΔT is small, track slabs with a shorter l_0 are more prone to up-warp displacement. When ΔT is large, track slabs with a longer l_0 have a greater up-warp displacement. For ΔT ranges in 0–17, 17–30, or 30–60 °C, the l_0 value corresponding to the maximum value of f is about 3, 5, or 6.5 m, respectively. Therefore, during the process of construction and maintenance, the value of l_0 should be strictly controlled to be less than 6.5 m.

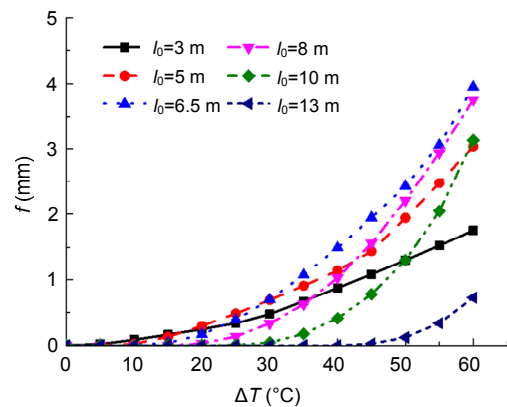


Fig. 16 Variation in f under different values of l_0

Fig. 17 shows that the variation law between the maximum value of l and l_0 is similar to that of the case of the maximum value of f . For ΔT ranges in 0–10, 10–17, 17–30, 30–45, or 45–60 °C, the l_0 value corresponding to the maximum value of l is about 3, 5, 6.5, 8, or 13 m, respectively. The ratios (f/l) of track slabs under different values of l_0 with the condition of ΔT ranging in 0–60 °C are shown in Table 4.

According to Table 4, if ΔT is in the range of 40–60 °C, the ratio (f/l) reaches a maximum on track slabs with $l_0=6.5$ m.

Fig. 18 shows that when l_0 reaches 6.5 m, M_a is the largest. If l_0 exceeds 6.5 m, constrained by gravitational field, l does not reach the value of l_0 , f_0 begins to decrease, and M_a decreases accordingly. When l_0 is about 6.5 m, the concrete pressure at the apex is the most unfavorable. In addition, when l_0 is less than

6.5 m, M_a is also close to the critical value of 98.6 kN·m. Therefore, an extra attention should be paid to l_0 with a span length of less than one slab.

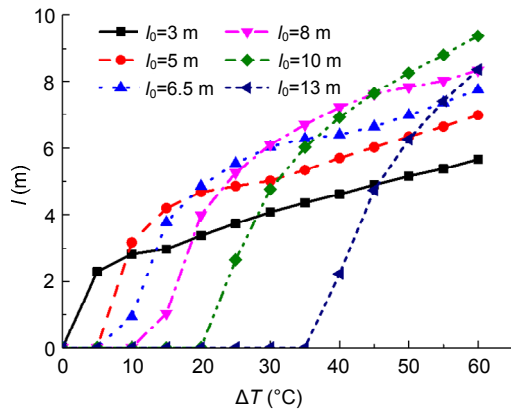


Fig. 17 Variation in l under different values of l_0

Table 4 Ratios (f/l) under different values of l_0

ΔT (°C)	f/l (mm/m)					
	$l_0=3$ m	$l_0=5$ m	$l_0=6.5$ m	$l_0=8$ m	$l_0=10$ m	$l_0=13$ m
10	0.03	0.01	0.01	0	0	0
20	0.07	0.06	0.03	0.01	0	0
30	0.12	0.14	0.12	0.05	0.01	0
40	0.19	0.20	0.23	0.14	0.06	0.01
50	0.25	0.31	0.35	0.28	0.16	0.02
60	0.31	0.44	0.54	0.45	0.33	0.09

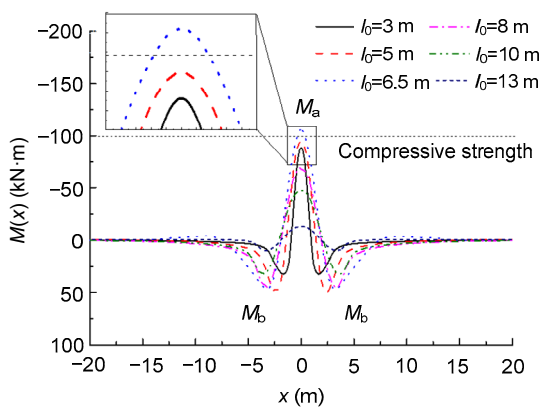


Fig. 18 Distribution of $M(x)$ under different values of l_0 ($\Delta T=60$ °C)

5.3 Effects of line types of initial up-warp on the stability of track slabs

The practice has shown that factors affecting wide-narrow joints after pouring construction lead to different line types of initial up-warp. To study the

deformation regulation of up-warp with different line types, five typical primary initial up-warp lines of track slabs were assumed: primary sine curve, quadratic sine curve, cubic sine curve, circular curve, and angular curve (Fig. 19). Among them, both the first and second derivatives of the quadratic and cubic sine curves are continuous at the boundary. According to Fig. 19, the primary sine curve and circular curve are smooth at the apex, but there are angles at the boundaries, and the angle at the boundary is larger for a circular curve. According to the calculation above, assuming that $f_0=15$ mm and $l_0=6.5$ m, the results for f are as shown in Fig. 20, those for up-warp regulation of l are shown in Fig. 21, and those for $M(x)$ under the condition of $\Delta T=60$ °C are shown in Fig. 22.

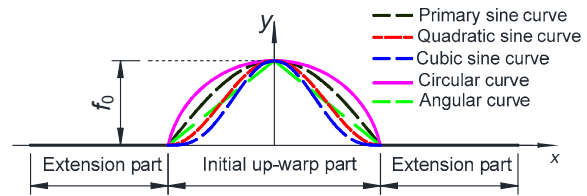


Fig. 19 Diagram of line types of initial up-warp (References to color refer to the online version of this figure)

Fig. 20 shows that when $\Delta T=60$ °C, the values of f for primary sine, quadratic sine, cubic sine, circular, and angular curves are 4.4, 4.2, 3.9, 4.6, and 3.6 mm, respectively. An angular curve line type can restrict track slab up-warp to a certain extent because the angle at the apex bears two sides of temperature loads. Therefore, the track system is slightly more stable. With angles at boundaries becoming larger, the value of f is larger for primary sine and circular curves. In addition, with a larger index of the sine curve, boundaries become smoother, and constraints at the end become stronger; therefore, the track system becomes more stable.

Fig. 21 shows that the values of l are closely related to the line types of the initial up-warp. For the initial line types with an angle at the apex, a small temperature rise can cause local de-bonding at the bottom of the track slab. However, l increases slightly with the increase of ΔT before l reaches l_0 . From the cases of the circular curve and primary sine curve, with the angle at the boundary becoming larger, the degree of ΔT that causes the local de-bonding at the bottom of track slab becomes lower. For line types

without angles at the apex, like quadratic and cubic sine curves, with the increase of ΔT , if the boundary is smoother, l is shorter. When $\Delta T=60^\circ\text{C}$, the values of l for the quadratic sine, cubic sine, and angular curve cases are smaller compared to those for circular and primary sine curves, which are 7.74, 7.41, and 7.62 m, respectively. Therefore, track slabs with an angle at the apex or smooth boundaries of initial up-warp more easily maintain their original form.

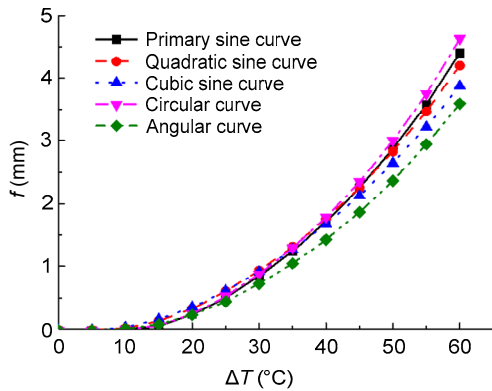


Fig. 20 Variation in f under different line types of initial up-warp

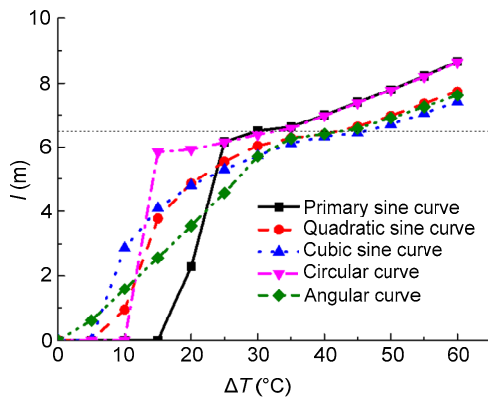


Fig. 21 Variation in l under different line types of initial up-warp

Fig. 22 shows that for line types of initial up-warp with an angle at the apex, or smooth boundaries, M_b is smaller. In addition, if line types have a smoother boundary, l is shorter and M_a is more concentrated. Among the line types, for quadratic and cubic sine curves, M_a exceeds the critical value of 98.6 kN·m. Therefore, pressure failure is more prone to occur on the bottom slab of an apex with a smoother initial up-warp.

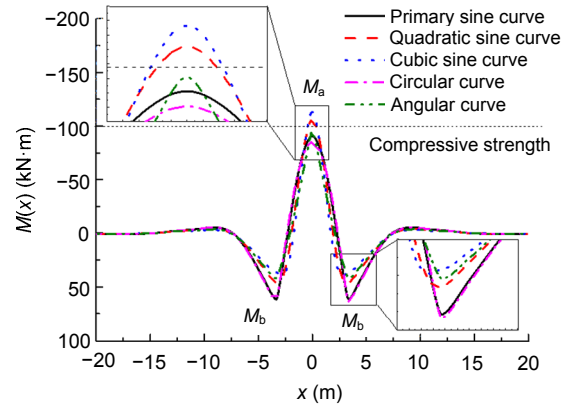


Fig. 22 Distribution of $M(x)$ under different line types of initial up-warp ($\Delta T=60^\circ\text{C}$)

6 Conclusions

1. The trend in f was almost the same when estimated by FEM, analytical method, or on-site testing, but there was a better agreement between the FEM and the analytical method. The error of f from the test result was maintained within the range of 0.1 mm in the stage of elastic deformation, and the error of P_{cr} was almost within the range of 10%.

2. Early processes of construction and operation would not induce instability in the track system. If l_0 remained unchanged, the ratio (f/l) would become larger with a greater value of f_0 .

3. If track slabs remained with $l_0=6.5$ m, when f_0 exceeds 15 mm, concrete at the bottom of the apex was most susceptible to compressional destruction. In high-temperature environments, the ratio (f/l) was at its maximum when $l_0 =6.5$ m.

4. Slabs which have line types of initial up-warp that have angles at the apex or have smooth boundaries more easily maintained their original form under high temperatures. However, concrete at the bottom of the apex was more prone to pressure failure if track slabs have smooth boundaries.

References

Cao SH, Yang RS, Su CG, et al., 2016. Damage mechanism of slab track under the coupling effects of train load and water. *Engineering Fracture Mechanics*, 163:160-175. <https://doi.org/10.1016/j.engfracmech.2016.07.005>

Crisfield MA, 1982. Accelerated solution techniques and concrete cracking. *Computer Methods in Applied Mechanics and Engineering*, 33(1-3):585-607.

- [https://doi.org/10.1016/0045-7825\(82\)90124-4](https://doi.org/10.1016/0045-7825(82)90124-4)
- Esveld C, 2001. Modern Railway Track (2nd Edition). MRT-Productions, Zaltbommel, the Netherlands, p.194-201.
- Fang YT, 2011. On China's high-speed railway technology. *Journal of Zhejiang University-SCIENCE A (Applied Physics & Engineering)*, 12(12):883-884. <https://doi.org/10.1631/jzus.A11GT000>
- Gao L, Liu YN, Zhong YL, et al., 2016. Influence of damage of wide and narrow joints on mechanical performance of CRTS II slab-type ballastless track CWR. *Railway Engineering*, 56(5):58-63 (in Chinese).
- Han J, Zhao GT, Xiao XB, et al., 2015. Effect of softening of cement asphalt mortar on vehicle operation safety and track dynamics. *Journal of Zhejiang University-SCIENCE A (Applied Physics & Engineering)*, 16(12):976-986. <https://doi.org/10.1631/jzus.A1500080>
- Kish A, Samavedam G, Jeong D, 1982. Analysis of Thermal Bucking Tests on U.S. Railroads. Technique Report No. NTIS-PB83-203554, Office of Research and Development, Federal Railroad Administration, US, p.21-102.
- Lichtberger B, 2005. Track Compendium: Formation, Permanent Way, Maintenance, Economics. Eurail Press, Hamburg, Germany, p.309-331.
- Lin N, Park N, Kang Y, 2003. Stability of continuously welded track. *Computers & Structures*, 81(22-23):2219-2236. [https://doi.org/10.1016/S0045-7949\(03\)00287-6](https://doi.org/10.1016/S0045-7949(03)00287-6)
- Liu FS, Zeng ZP, Wu B, 2015. Research on the CRTS II slab ballastless track buckling deformation in the process of construction. *Journal of Railway Engineering Society*, 32(1):55-60 (in Chinese).
- Liu XY, Zhao PR, Yang RS, et al., 2010. Design Theory and Method of Ballastless Track of Passenger Dedicated Railways. Southwest Jiaotong University Press, Chengdu, China, p.1-24 (in Chinese).
- Liu Y, Feng J, 2016. Treatment of upheaval of CRTS II-type ballastless track slab for Beijing-Tianjin intercity railway. *Railway Engineering*, 56(2):142-145 (in Chinese).
- Long G, Liu H, Ma K, et al., 2018. Development of high performance self-compacting concrete applied for filling layer of high-speed railway. *Journal of Materials in Civil Engineering*, 30(2):04017268. [https://doi.org/10.1061/\(ASCE\)MT.1943-5533.0002129](https://doi.org/10.1061/(ASCE)MT.1943-5533.0002129)
- Mallardo V, Alessandri C, 2004. Arc-length procedures with BEM in physically nonlinear problems. *Engineering Analysis with Boundary Elements*, 28(6):547-559. <https://doi.org/10.1016/j.enganabound.2003.11.002>
- Martinez IN, Sanchis IV, Fernandez PM, et al., 2015. Analytical model for predicting the buckling load of continuous welded rail tracks. *Proceedings of the Institution of Mechanical Engineers Part F: Journal of Rail & Rapid Transit*, 229(5):542-552. <https://doi.org/10.1177/0954409713518039>
- Reissner E, 1946. Analysis of shear lag in box beams by the principle of minimum potential energy. *Quarterly of Applied Mathematics*, 4(3):268-278.
- Ren JJ, Deng SJ, Jin ZB, et al., 2017. Energy method solution for the vertical deformation of longitudinally coupled prefabricated slab track. *Mathematical Problems in Engineering*, 2017(1):1-11. <https://doi.org/10.1155/2017/8513240>
- Rybkin V, Nastechikn MP, Nastechik NP, et al., 2013. Stability issues of the continuous welded rail track on the concrete sleepers on the curves with radius $R \leq 300$ m. *Sciences in Cold & Arid Regions*, 5(5):654-658. <https://doi.org/10.3724/SP.J.1226.2013.00654>
- Shahba A, Rajasekaran S, 2012. Free vibration and stability of tapered Euler-Bernoulli beams made of axially functionally graded materials. *Applied Mathematical Modelling*, 36(7):3094-3111. <https://doi.org/10.1016/j.apm.2011.09.073>
- Tan P, Ma JE, Zhou J, et al., 2016. Sustainability development strategy of China's high-speed rail. *Journal of Zhejiang University-SCIENCE A (Applied Physics & Engineering)*, 17(12):923-932. <https://doi.org/10.1631/jzus.A1600747>
- Tao GQ, Du X, Zhang HJ, et al., 2017. Development and validation of a model for predicting wheel wear in high-speed trains. *Journal of Zhejiang University-SCIENCE A (Applied Physics & Engineering)*, 18(8):603-616. <https://doi.org/10.1631/jzus.A1600693>
- Wei H, 2014. Research on the Track Irregularities Survey Theory and Relevant Adjustment Technologies of HSR Track. PhD Thesis, Nanchang University, Nanchang, China, p.18-22 (in Chinese).
- Yan B, Dai GL, Guo WH, et al., 2015. Longitudinal force in continuously welded rail on long-span tied arch continuous bridge carrying multiple tracks. *Journal of Central South University*, 22(5):2001-2006. <https://doi.org/10.1007/s11771-015-2721-5>
- Yang JB, Zeng Y, Liu XY, et al., 2015. Stability of CRTS-II slab track based on energy norm. *Journal of Central South University (Science and Technology)*, 46(12):4707-4712 (in Chinese).
- Zhang J, Xiao XB, Sheng XZ, et al., 2017. Characteristics of interior noise of a Chinese high-speed train under a variety of conditions. *Journal of Zhejiang University-SCIENCE A (Applied Physics & Engineering)*, 18(8):617-630. <https://doi.org/10.1631/jzus.A1600695>
- Zhang XM, Chen XF, 2007. A convenient computational method for analyzing the stability of continuously welded rail tracks. *Journal of the China Railway Society*, 29(1):124-126 (in Chinese).
- Zhang XM, Zhao L, 2018. Research on the stability theory of CRTS II slab ballastless track on high-speed railway. *Journal of Railway Engineering Society*, 35(1):49-55 (in Chinese).
- Zhao GT, 2010. Manufacturing technology of CRTS II ballastless track slab. *Railway Construction Technology*, 6:62-65 (in Chinese).

Zhou M, Dai GL, 2015. Stability of longitudinally connected ballastless slab track on simply-supported beam bridges of high-speed railway. *Journal of the China Railway Society*, 37(8):60-65 (in Chinese).

Ziegler H, 1977. *Principle of Structure Stability* (2nd Edition). Birkhäuser, Basel, Switzerland, p.1-32.

中文概要

题目: 初拱变形对 CRTS II 型板式轨道高温稳定性影响研究

目的: 初拱变形是影响 CRTS II 型板式轨道垂向稳定性的关键因素之一。通过建模分析, 深入研究初拱变形的不同特征量, 即矢度、弦长和线型, 对其受力变形及高温稳定性的影响。

方法: 基于变波长变形曲线建立 CRTS II 型板垂向稳定

性分析理论, 开展缩尺模型试验验证, 并通过有限元法进行计算仿真。

结论: 有限元法、解析法与现场试验所得垂向上拱位移的变化趋势一致, 有限元法与解析法结果吻合更好。轨道板初拱弦长为 6.5 m 且初拱矢度超过 15 mm 时, 拱顶处下缘混凝土最易发生受压破坏。在高温环境下, 初拱弦长为 6.5 m 的轨道板上拱矢跨比最大。拱顶存在折角、初拱段边界平滑的轨道板在高温环境下更容易保持原有形态, 但后者于拱顶处下缘的混凝土更容易发生受压破坏。故为确保 CRTS II 型板的稳定性, 应避免弦长达 6.5 m 且矢度超过 15 mm 的初始上拱, 另需关注不同初拱线型对轨道板上拱的影响。

关键词: 高速铁路; CRTS II 型板式轨道; 初拱变形; 高温; 稳定性